Electronic Supplementary Material (ESI) for Journal of Materials Chemistry A.
This journal is © The Royal Society of Chemistry 2020

Supporting Information

Effect of grain size on electrochemical performance and kinetics of Co_3O_4 electrode material

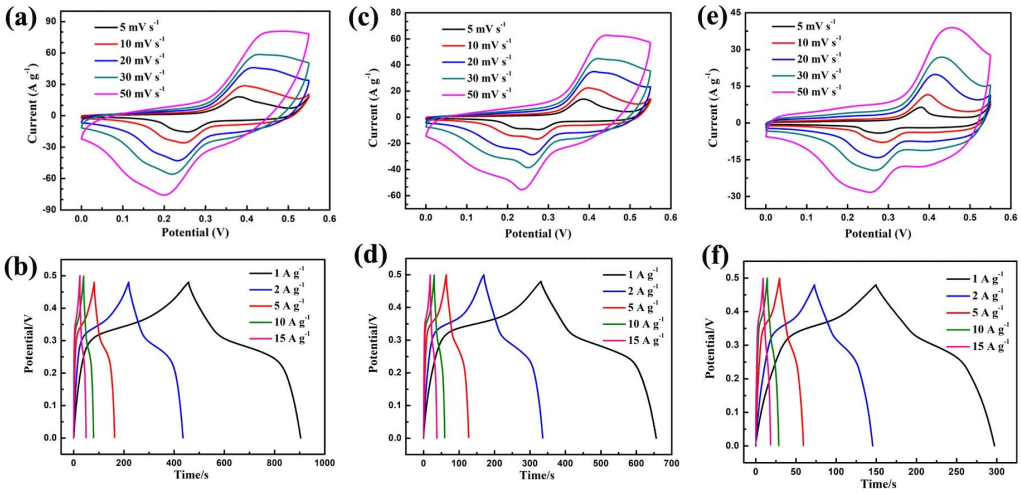

Fig. S1 Electrochemical performance for Co_3O_4 samples. (a, b) Co_3O_4-300; (c, d) Co_3O_4-350; (e, f) Co_3O_4-400.

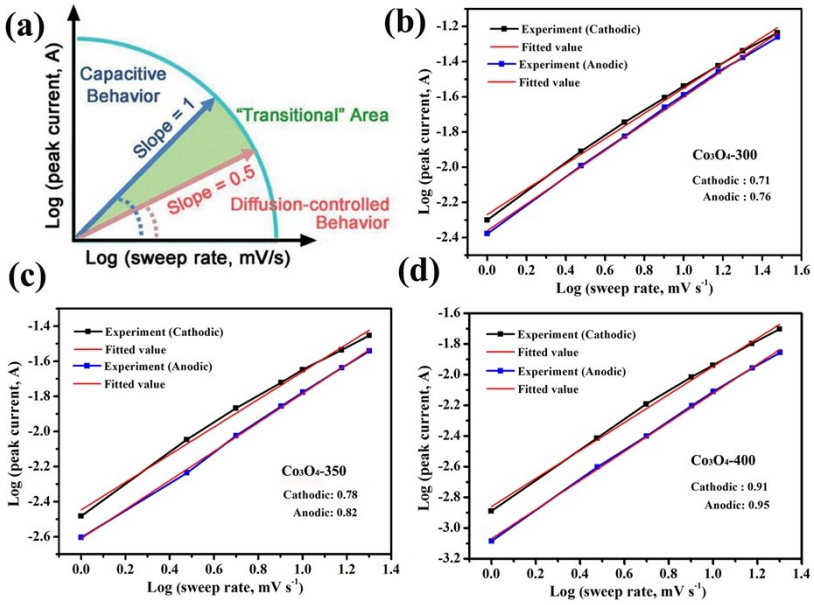

Fig. S2 (a) Power law dependence of the peak current on sweep rate;[1] (b-d) Logarithmic curves of

the sweep rate and peak current for the cathodic and anodic, which can gives the *b* value.

In the CV test, the total current response measured at a certain sweep speed can be divided into two parts: one is the current generated by the slow diffusion-controlled process (i_{diff}), and the other is the current caused by the electric double layer or the fast Faraday reaction occurring on the electrode surface (i_{cap}). The specific empirical formula can be expressed as: [2-4]

$$i(v) = i_{cap} + i_{diff} = av^b \tag{3}$$

$$logi(v) = loga + blogv \tag{4}$$

Where *i* the peak current (A), *v* sweep rate (mv s^{-1}), a and b are the adjustment parameters. The value of b is obtained from a linear curve of log (*i*) *vs* log (*v*), which can provide kinetic information of electrochemical reaction for the electrode material. As shown in Fig. S2a, according to the *b* value, there are two well-defined conditions, $b = 0.5$ and $b = 1$. When $b \geq 1$, it means that the current contribution is completely derived from the capacitive contribution, such as an electric double layer during charge and discharge or a rapid surface redox reaction; When $b \leq 0.5$, it means that all of the current contribution comes from the semi-infinite diffusion control process, namely battery type materials. [5-8] If b is between 0.5-1, it indicates that the electrode material is in the transition region between battery and capacitance. Fig. S2b-d give the b value of the Co_3O_4 materials in different annealing temperature. For Co_3O_4-300, 350 and 400, the b value of cathodic is 0.71, 0.78 and 0.91, respectively. For anodic, the values of b also have a visible rise with the increase of annealing temperature. This means that the

energy storage behaviour of electrode materials tends to capacitive behavior, and the diffusion control behaviour is gradually reduced with the increase of annealing temperature.

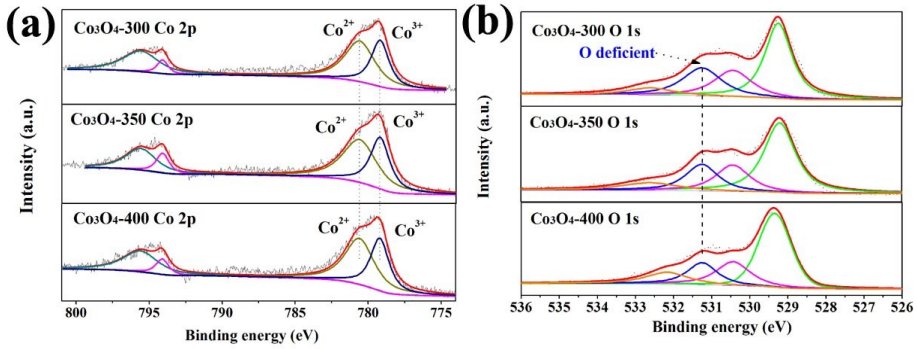

Fig. S3 XPS spectrum for different Co_3O_4 electrode. (a) Co 2p; (b) O 1s.

Fig. S3a displayed the Co 2p spectrums for different Co_3O_4 samples. All peaks can be further divided into four peaks, which correspond to Co elements with different valence states. There are two distinct emission peaks at the bond energy of about 700 eV and 796 eV, which belong to the Co $2p_{3/2}$ and Co $2p_{1/2}$ orbitals respectively. The Co $2p_{3/2}$ can be further divided into two peaks located at 780.5 eV and 779.2 eV, which represent the spin-coupled doublet of Co^{2+} and Co^{3+} ions, respectively.[9,10] For O 1s spectrums as shown in Fig. S3b, they all can be decomposed into four peaks located at 529.2 eV, 530.4 eV, 531.3 eV and 532.4 eV, which representing oxygen atoms in the crystal lattice, low oxygen coordination defects, surface adsorption of oxygen atoms or hydroxyl oxygen, and oxygen atoms adsorbing molecular water, respectively.[10,11]

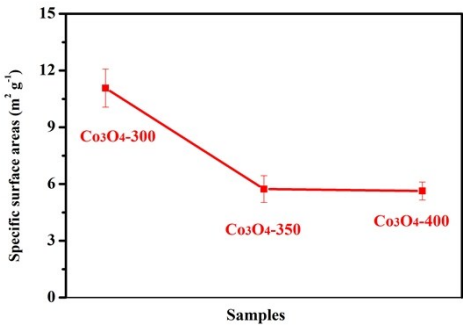

Fig. S4 The specific surface areas for the Co_3O_4-300, 350 and 400.

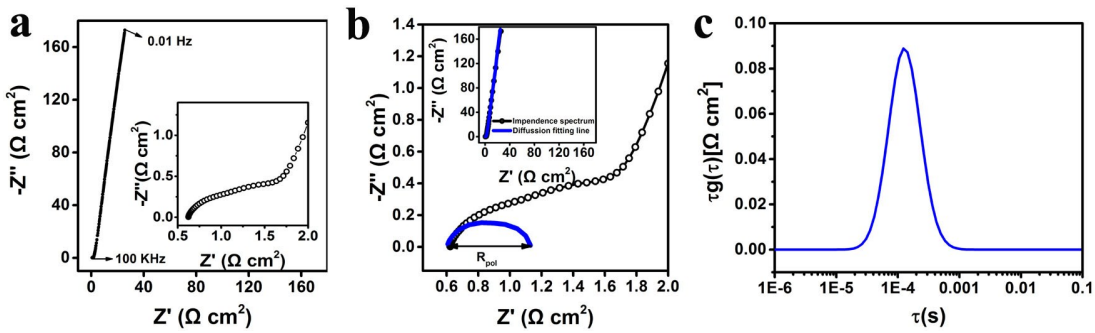

Fig. S5 (a) EIS of Co_3O_4-300 electrode tested at 25℃ (b) $Z_{pre}(\omega)$ (blue line) after subtraction, inset: diffusion branch modeled by GFSW element (blue line) and (c) corresponding DRT result of $Z_{pre}(\omega)$ in (b).

For supercapacitors, the impedance can be expressed by the following equation: [12]

$$Z(\omega) = R_0 + Z_{pol}(\omega) + Z_{diff} = R_0 + \int_0^{\infty} \frac{g(\tau)}{1 + j\omega\tau} d\tau + Z_{diff} \tag{1}$$

where $g(\tau)$ is the DRT function, $g(\tau)d\tau$ and $\tau/g(\tau)d\tau$ are the corresponding polarization resistance and capacitance for each polarization process. Here, $g(\tau)$ satisfies the following boundary condition:

$$\int_0^{\infty} \frac{g(\tau)}{1 + j\omega\tau} d\tau = Z'(0) - Z'(\infty) \tag{2}$$

The diffusion branch Z_{diff} should be firstly subtracted from $Z(\omega)$ since it is mathematically divergent. Here, a commonly used generalized finite-space Warburg (GFSW) element is used to model Z_{diff} in the case of reflective boundary condition [13,14]. Therefore, Z_{diff} in equation (1) is expressed as:

$$Z_{diff} = R_w \frac{coth\left[(j\omega\tau_d)^p\right]}{(j\omega\tau_d)^p} \tag{3}$$

Where R_w is the polarization resistance of diffusion process, p is a constant in the range from 0 to 1, τ_d is the relaxation time of diffusion process defined as l^2/D_{eff}, where l is the finite diffusion length (electrode thickness) and D_{eff} is the effective diffusivity. After subtraction of Z_{diff}, the resulted impedance ($Z_{pre}(\omega)$), which is appropriate for DRT analysis, can be expressed as:

$$Z_{pre}(\omega) = R_0 + Z_{pol}(\omega) = Z(\omega) - Z_{diff} = R_0 + \int_0^{\infty} \frac{g(\tau)}{1 + j\omega\tau} d\tau \tag{4}$$

Fig. S5 gives an example of the diffusion branch model and subtraction of Co_3O_4-300. Fig. S5a shows the original EIS of Co_3O_4-300 obtained at 25℃. Generally, the curve can be divided into three parts, namely a high frequency interception, an intermediate-frequency region and a low-frequency region, representing the equivalent series resistance of the electrode material, the charge transfer across the electrode/electrolyte interface, and the ions diffusion process in bulk electrode materials, respectively. The diffusion branch is well modeled by GFSW element (inset of Fig. S5b, blue line) and the converged $Z_{pre}(\omega)$ obtained after subtraction of Z_{diff} are shown in Fig. S5b (blue lines). The corresponding DRT result of $Z_{pre}(\omega)$ in Fig. S5b is shown in Fig. S5c. The

result shows one sub-process with relaxation time of about 1.0×10^{-5} s -5.0×10^{-5} s in high frequency region, and this relaxation process should be ascribed to the charge transfer across the Co_3O_4/electrolyte interface since it is the only possible rate determining process in high frequency region.

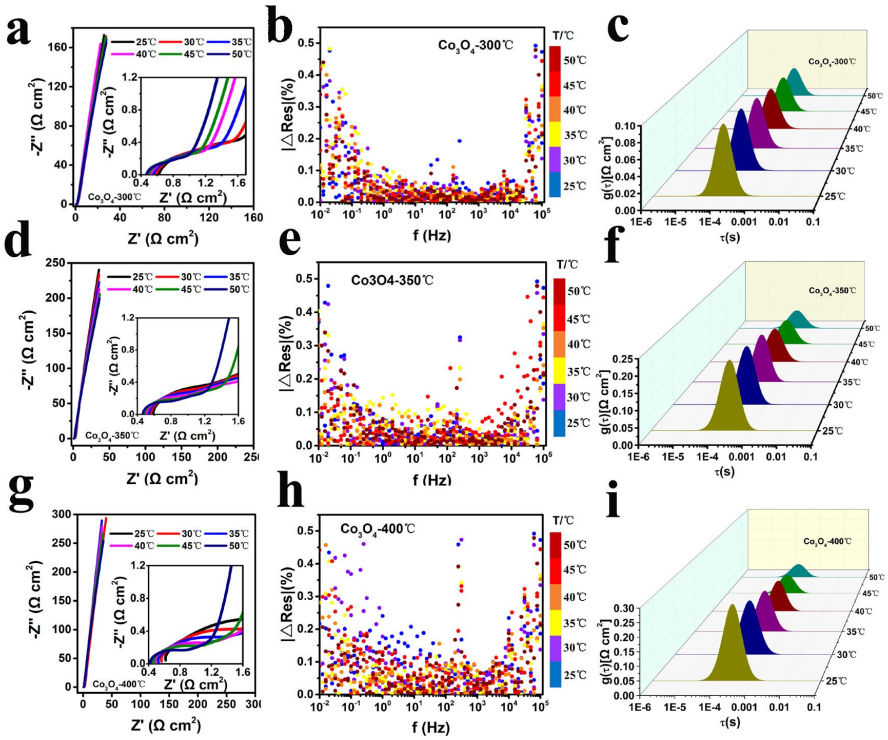

Fig. S6 (a, d, g) EIS date for Co_3O_4-300, Co_3O_4-350, Co_3O_4-400 electrode tested at 25ºC, 30ºC, 35ºC, 40ºC, 45ºC, 50ºC, respectively; (b, e, h) Absolute residuals of real and imaginary part of different samples; (c, f, i) the DRT result for Co_3O_4 samples;

EIS date for three samples obtained at different temperatures (25ºC, 30ºC, 35ºC, 40ºC, 45ºC, 50ºC) and absolute residuals of real and imaginary part, calculated according to Kramers-Kronig relation, were shown in Fig. S6. Residuals for all EIS are well below 0.5% in 0.01-100 kHz, indicating very high data quality of all EIS spectra. Fig. S6c, f and i show the DRT results of all six impedances obtained at 25℃, 30℃,

35℃, 40℃, 45℃and 50℃, respectively.

Calculation of resistance (R) values of diffusion process (P_{diff}) and charge transfer process (P_{ct}):

Equation (3) represents the model of generalized finite-space Warburg (GFSW) element in diffusion process. The resistance value of the diffusion process in this paper is obtained by fitting the diffusion branch using equation (3). Resistance value of the charge transfer process is obtained by calculating the peak area in DRT curve (Figure S6c, S6f, and S6i).

Tab. S1 Capacitive contribution and diffusion contribution at different sweep rate for different Co_3O_4 samples.

300℃	**Sweep rate (mV s^{-1})**	**0.5**	**0.8**	**1**	**3**	**5**
	Total capacitance (C g^{-1})	**486**	**476**	**470**	**463**	**457**
	Surface capacitance (C g^{-1})	**435**	**435**	**435**	**435**	**435**
	Diffusion contribution (C g^{-1})	**51**	**41**	**35**	**28**	**22**
350℃	**Sweep rate (mV s^{-1})**	**0.5**	**0.8**	**1**	**3**	**5**
	Total capacitance (C g^{-1})	**363**	**352**	**353**	**347**	**343**
	Surface capacitance (C g^{-1})	**333**	**333**	**333**	**333**	**333**
	Diffusion contribution (C g^{-1})	**30**	**19**	**20**	**14**	**10**
400℃	**Sweep rate (mV s^{-1})**	**0.5**	**0.8**	**1**	**3**	**5**
	Total capacitance (C g^{-1})	**165**	**163**	**162**	**164**	**163**
	Surface capacitance (C g^{-1})	**162**	**162**	**162**	**162**	**162**
	Diffusion contribution (C g^{-1})	**3**	**1**	**0**	**2**	**1**

Reference

1. J. Liu, J. Wang, C. Xu, H. Jiang, C. Li, L. Zhang, J. Lin and Z. X. Shen, *Advanced science*, 2018, **5**, 1700322.

2. D. Baronetto, N. Krstajić and S. Trasatti, *Electrochimica acta*, 1994, **39**, 2359-2362.

3. M. Sathiya, A. Prakash, K. Ramesha, J. M. Tarascon and A. K. Shukla, *Journal of the American Chemical Society*, 2011, **133**, 16291-16299.

4. H. Lindström, S. Södergren, A. Solbrand, H. Rensmo, J. Hjelm, A. Hagfeldt and S.-E. Lindquist, *The Journal of Physical Chemistry B*, 1997, **101**, 7717-7722.

5. V. Augustyn, J. Come, M. A. Lowe, J. W. Kim, P.-L. Taberna, S. H. Tolbert, H. D. Abruña, P. Simon and B. Dunn, Nature materials, 2013, 12, 518-522.

6. J. Come, P.-L. Taberna, S. Hamelet, C. Masquelier and P. Simon, *Journal of The Electrochemical Society*, 2011, **158**, A1090-A1093.

7. J. Wang, J. Polleux, J. Lim and B. Dunn, *The Journal of Physical Chemistry C*, 2007, **111**, 14925-14931.

8. M. Sathiya, A. Prakash, K. Ramesha, J. M. Tarascon and A. K. Shukla, *Journal of the American Chemical Society*, 2011, **133**, 16291-16299.

9. Y. Wang, T. Zhou, K. Jiang, P. Da, Z. Peng, J. Tang, B. Kong, W. B. Cai, Z. Yang and G. Zheng, *Advanced Energy Materials*, 2014, **4**, 1400696.

10. L. Zhuang, L. Ge, Y. Yang, M. Li, Y. Jia, X. Yao and Z. Zhu, *Advanced Materials*, 2017, **29**, 1606793.

11. Y. Zeng, Y. Han, Y. Zhao, Y. Zeng, M. Yu, Y. Liu, H. Tang, Y. Tong and X. Lu, *Advanced energy materials*, 2015, **5**, 1402176.

12. W. Li, Y. Li, X. Yao, M. Fang, M. Shui, J. Shu and Y. Ren, *Bulletin of Materials Science*, 2018, **41**, 155.

13. C. Gabrielli, P. Grand, A. Lasia and H. Perrot, *Journal of The Electrochemical Society*, 2004, **151**, A1925-A1936.

14. L. Birry and A. Lasia, *Electrochimica acta*, 2006, **51**, 3356-3364.